Intertwined Multiple Spiral Fracture in Perforated Sheets

Juan-Francisco Fuentealba,[1] Eugenio Hamm,[1,*] and Benoît Roman[2]
[1]Departamento de Física, Universidad de Santiago de Chile, Avenida Ecuador 3493, 9170124 Estación Central, Santiago, Chile
[2]PMMH, CNRS UMR 7636, UPMC, Université Paris 6 and Université Paris Diderot Paris 7, ESPCI Paris, 10 rue Vauquelin, 75231 Paris Cedex 05, France

(Received 22 January 2016; revised manuscript received 28 March 2016; published 20 April 2016)

We study multiple tearing of a thin, elastic, brittle sheet indented with a rigid cone. The n cracks initially prepared symmetrically propagate radially for $n \geq 4$. However, if $n < 4$ the radial symmetry is broken and fractures spontaneously intertwine along logarithmic spiral paths, respecting order n rotational symmetry. In the limit of very thin sheets, we find that fracture mechanics is reduced to a geometrical model that correctly predicts the maximum number of spirals to be strictly 4, together with their growth rate and the perforation force. Similar spirals are also observed in a different tearing experiment (this time up to $n = 4$, in agreement with the model), in which bending energy of the sheet is dominant.

DOI: 10.1103/PhysRevLett.116.165501

We are all familiar with the star-shaped radial fracture patterns on a broken window after impact, which may even present secondary circumferential cracks for sufficiently high impact speed [1]. However, the perforation of solid plates is of interest for security applications [2], the stability of structures on ice sheets [3], and in forensic studies [4], but also for computer graphics [5]. More generally, the complex crack trajectories during impact on brittle solids define the size and shape of the fragments [6,7] and are relevant for the crushing processes in industry. In a rationalizing approach, several studies focus on the quasistatic version of perforation-induced fracture in aluminium foils, where the final number n of radial cracks is attained either by halting or splitting events [1,8].

In this Letter, we study experimentally and theoretically the crack patterns due to quasistatic perforation of a brittle sheet by a rigid cone. We use polypropylene sheets, in which crack initiation and splitting are not possible for the typical stresses reached during perforation. Starting from a large number n of initial radial notches, cracks propagate along straight radial lines. However, for a sufficiently small n, we observe tears that spontaneously swirl one around the other. This pattern has been reported once [6] but never studied. This unexpected behavior challenges numerical and theoretical modeling, which usually assumes radial propagation and petaling patterns [9]. We also observe similar multiple spiral patterns when pulling the flaps in between notches perpendicularly from the plane of the sheet, as in Ref. [10]. Although spiral fracture patterns have been observed in coatings under residual tensile stresses [11–16] and interacting cracks mutually curving their paths under uniaxial tension [17], the spirals reported here are of a very different nature. Indeed, they involve the interaction of several cracks through large out-of-plane bending, and they appear after breaking the radial symmetry of the loading.

We give a theoretical description of the crack path based on basic principles of fracture mechanics in very thin brittle sheets [18]. This leads us to a purely geometrical problem where the existence and shape of multiple spiral cracks can be explained in terms of a delayed crack interaction. We examine the maximum number of spiral arms, and we compare the measured and predicted tearing forces for the spiral and radial modes.

Experimental setup.—We tear bioriented polypropylene sheets (Innovia, 30–90 μm thick, fracture energy $G_c \sim 10$ KJ/m^2), which are brittle and fairly isotropic [19]. Sheets are prepared with a series of n regularly distributed radial notches of length (7 ± 1) mm. We use two setups (Fig. 1). *Pushing* setup: sheets are fixed to a rigid frame (size 48×50 cm^2) and pierced quasistatically (speed 12.5 mm/s) with a circular cone (opening angle $2\gamma = 45.2°$). A load cell records the force F applied on the cone. *Pulling* setup: the radial notches are conveniently modified for easy gripping of the flaps between the notches. The flaps are pulled perpendicularly away from the plane of the sheet (see also Ref. [10]), with a constant speed in the range 1–10 mm/s. Both setups lead to the propagation of exactly n cracks during the experiment, with propagation speed within the range 1–60 mm/s. Variations within this range did not alter the results in an appreciable way.

In both experiments, we observe radial fracture patterns (Fig. 1) when starting from $n \geq 4$ notches, thus preserving the n-rotational symmetry, but also the n planar reflections with respect to each of the rectilinear cuts. However, for $n < 4$ (and in some cases also for $n = 4$ in the pulling configuration) an intriguing chiral spiraling pattern spontaneously develops. Figure 2 shows the polar representation $r(\theta)$ of the crack paths, from scanned samples. The paths are reproducible, and the n spiral branches collapse on a single curve which promptly converges to a logarithmic

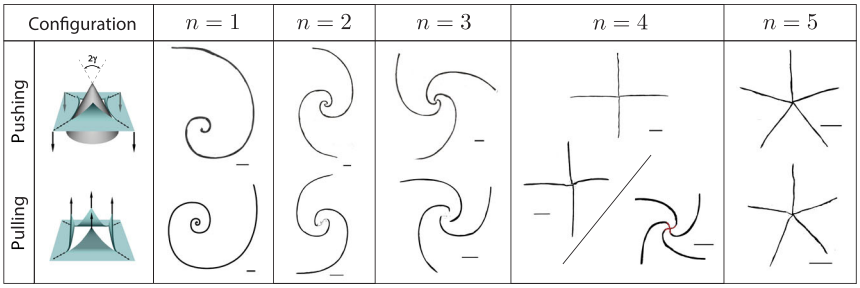

FIG. 1. Scanned crack paths obtained for $n = 1$ to 5 initial radial notches (sheet thickness 30 μm). Upper and lower rows correspond respectively to the pushing (2γ is the opening angle of the cone) and pulling configurations (shown are $n = 4$ initial radial notches). In the pulling case for $n = 4$, spirals are obtained if notches are S shaped. Horizontal bars in each subfigure are 5 cm long.

spiral $r(\theta) \propto \exp(\sigma\theta)$, where σ is a constant that determines the spiral's rate of growth. This convergence is more efficient for large n's, and for $n = 1$ it takes roughly three quarters of a turn to reach the exponential behavior [10] [Fig. 2(a)]. A logarithmic spiral is characterized by a constant polar tangential angle, whose complement, ψ, is known as the spiral *pitch* and obeys $\sigma = \tan\psi$. In experiments, the spiral growth rate σ and the pitch increase with the number of cracks n [see Fig. 4(a)].

We first consider the pushing configuration. The cone acts in the plane of the sheet as an expanding disk that forces the film radially outwards. This configuration is a polar version of the straight cutting of a sheet with a blunt tool in which an oscillatory crack is observed [20]. A central area of the sheet (Fig. 1) is divided into n flaps which are free to bend away: this region is the convex hull of the reunion of all crack paths. In the case of radial propagation, this is a n polygon whose vertices are the n crack tips, and whose edges are lines around which the flaps strongly bend out of plane. The spiral case (Fig. 3) is more complex, as the boundary of the convex hull involves bending lines and portions of the cuts: the bending boundary originating from the crack tip A connects tangentially to the neighboring cut (in red) at point T. This line is broken into an angle α_c by the lateral force applied by the cone at contact point P [Fig. 3(d)].

Spiral paths in a zero elasticity model.—We assume in a first approximation [18] that the sheet is infinitely bendable and that fracture propagates before any noticeable in-plane strain builds up (see the below discussion of validity of this assumption). In this limit, the bending line remains straight (viz. $\alpha_c = 0$, and points A, P, T are aligned), and the convex hull must always encompass the expanding disk [Fig. 3(e)] by continuous propagation of the cracks.

To determine the direction of propagation of the crack tip when the radius ρ of the expanding disk increases by $d\rho$, we invoke the maximum energy release rate criterion [21]. Assuming no friction, and because the inextensible, infinitely bendable sheet may not store elastic energy, the work of the operator is in this model entirely dissipated in fracture energy and

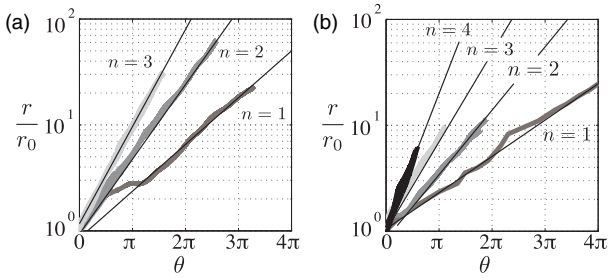

FIG. 2. Semilog plot of the n spiral crack paths in 30 μm thick sheets for (a) pushing and (b) pulling. The n rotated branches of the n spiral almost superpose in this graph. Straight lines evidence the exponential behavior.

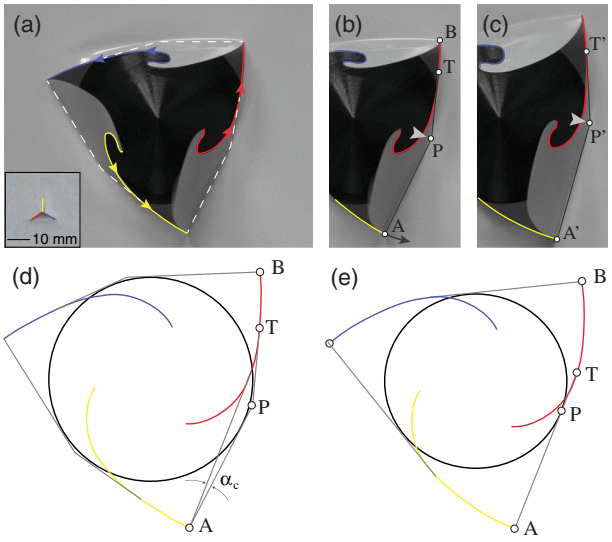

FIG. 3. Geometry of spiraling crack paths. (a) Perforation with a cone from a three-notch initial condition (inset), forms a three-spiral pattern (crack paths and "bending lines," respectively, in color and dashed lines). (b),(c) Sequence of crack propagation (A to A'): contact point with the cone (arrowhead) moves from P to P', and the tangency point from T to T'. (d) Elements of spiral tearing: the cone stretches the bending line APT until the crack at A starts to move. (e) Zero elasticity approximation: the bending line $\overline{AT}$ is straight, and the yellow crack path is the involute of the developed red crack path.

$$F dz = F \cot\gamma d\rho = n G_c t ds, \quad (1)$$

where F is the force applied on the cone, G_c is the fracture energy per unit surface, t is the thickness, and ds is the distance traveled by each crack. The energy release rate is maximum (or the operator's force F required for propagation is minimal) if the fracture proceeds in a direction where $ds/d\rho$ is minimal and hence in a direction perpendicular to the bending line $\overline{AT}$.

In the zero elasticity approximation, a crack path therefore obeys the following geometrical rule: in Fig. 3(e), the yellow crack path is the involute of the red crack path, as the former always intersects perpendicularly the tangents to the latter. A convenient way to define the involute is through its tangential angle φ, relative to a fixed arbitrary reference, and the instantaneous radius of curvature R at A, which obey (see the Supplemental Material [22]) $dR/d\varphi = \tilde{R}$, where $\tilde{R}$ is the radius of curvature of the reference curve at T.

For the sake of simplicity, we start with the case of $n = 1$, which amounts to seeking a curve which is the involute of itself. Given that T and A are on the same curve, we may write $\tilde{R} = R[\varphi - (3\pi/2)]$, which expresses the fact that the tangential angle rotates by $3\pi/2$ between T and A. The general case of n spirals is equivalent to n recursive involutes. If we assume n-rotational symmetry, the involutes are identical and share the same radius function $R(\cdot)$. The delay angle relating the point of tangency to the corresponding crack is now

$$\delta_n = \frac{\pi}{2n}(4 - n). \quad (2)$$

Only a positive delay, $\delta_n \geq 0$, corresponds to a physical fracture pattern because it ensures that point T lies on a part of the curve that has already been cut by the fellow fracture. We obtain the linear delay differential equation

$$\frac{dR}{d\varphi} = R(\varphi - \delta_n). \quad (3)$$

Real solutions of Eq. (3) exist in the form of exponentials,

$$R(\varphi) = S e^{\sigma\varphi}, \quad \text{where } \sigma \text{ obeys } \quad \sigma e^{\sigma\delta_n} = 1 \quad (4)$$

and S is an arbitrary scaling factor. The solution of Eq. (4) for σ can be expressed in terms of the Lambert W function [23] as $\sigma = W(\delta_n)/\delta_n$. Given that $W(\delta_n)$ is positive for $\delta_n > 0$ (i.e., $n < 4$), we conclude that our model correctly predicts a solution of the perforation problem where the crack paths are growing intertwined logarithmic spirals, as observed in the experiments. For $n = 4$ ($\delta_4 = 0$), the point T in Fig. 3(f) is exactly at the tip of the fellow crack. We conclude that only $n \leq 4$ spiral cracks are possible in the zero elasticity approximation.

Figure 4(a) shows that the prediction of the spiral growth rate, σ (the solid black line), is in good agreement with the experiments. As expected, σ is almost independent of the sheet thickness [Fig. 4(a) inset]. Pushing and pulling spirals are identical within the zero elasticity assumption [18]. However, we observe that the pulling spirals have systematically a lower growth rate than the pushing spirals, and that four-arm spirals are never obtained for the latter. We must examine the elastic energy of the plate to explain these discrepancies.

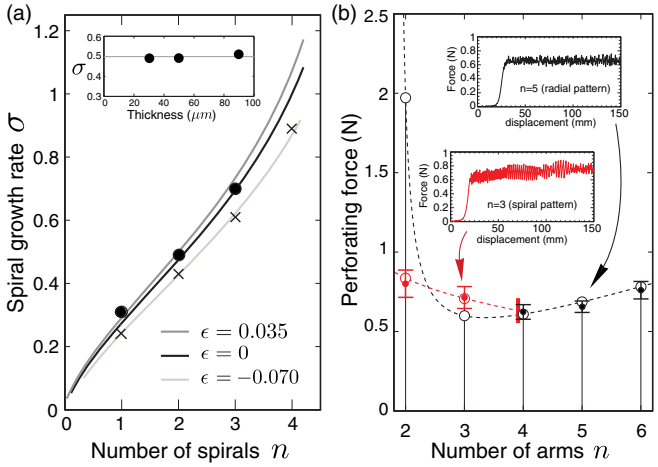

FIG. 4. (a) Spiral growth rate for pushing (circle) and pulling (times) experiments (30 μm sheets), and a comparison with Eq. (6) (lines). Values of ϵ are fitted separately for pushing and pulling. (Inset) Growth rate of a 2 spiral as a function of sheet thickness in a perforation experiment. (b) Perforation forces for spiral (red) and radial (black) patterns. Error bars, experiments with $t = 30$ μm thick sheets; open symbols, theoretical predictions after Eq. (7) with no adjustable parameters; dashed lines, theoretical predictions extended to noninteger values of n. The spiral solution (red, $\alpha_c = 6°$, $\epsilon = 0.035$, $G_c t = 0.206$ N) is observed only for $n < 4$, whereas the radial solution (black, $\alpha_c = 7°$, $G_c t = 0.288$ N) holds for $n \geq 4$.

Spiral path in a model including elasticity.—Elastic deformations of the plate in the vicinity of the bending line modify the direction of propagation of the cracks. In the pushing case, the bending line is broken [with an angle α_c; see Fig. 3(d)]—hence stretched—and may release energy by increasing its length [18]. In contrast, bending is dominant in the pulling case, and the release of energy occurs for a decrease of the length of the bending line [10,24]. This results in a deflection of propagation by an angle ϵ, counted positively here for pushing. It can be shown [18] that $\epsilon \sim (l_E/\ell)^{1/3}$ and $\epsilon \sim -(l_B/\ell)^{1/2}$ in the pushing or pulling case. Here, ℓ is the typical length of the bending line (several centimeters), whereas $l_E = G_c/E$ (E is the Young's modulus of the material) and $l_B = B/G_c t$ (B stands for bending stiffness) are characteristic length scales below which stretching and bending energy density, respectively, becomes comparable to the fracture energy G_c. In our experiments, $l_E \sim l_B \sim 10^{-5}$ m $\ll \ell$. This justifies the use of the zero elasticity model as a first approximation and suggests that $|\epsilon| \ll 1$. If we now assume that ϵ is

nonzero but constant (a reasonable approximation [10]), the cracks describe a *tanvolute* [25]. The generalization of Eq. (3) leads to (see the Supplemental Material [22])

$$\frac{d\ell(\varphi)}{d\varphi} = \frac{\ell(\varphi - \delta_n + \epsilon)}{\cos\epsilon} + \ell(\varphi)\tan\epsilon, \tag{5}$$

where $\ell(\varphi)$ is the length of the bending line. Equation (5) again has exponential solutions $\ell(\varphi) \propto e^{\sigma\varphi}$, with the growth rate

$$\sigma = \frac{1}{\delta_n - \epsilon} W\left(\frac{\delta_n - \epsilon}{\cos\epsilon} e^{-(\delta_n - \epsilon)\tan\epsilon}\right) + \tan\epsilon, \tag{6}$$

where the zero elasticity approximation corresponds to $\epsilon = 0$. In the limit of $|\epsilon| \ll 1$, Eq. (6) can be approximated as $\sigma = \sigma_0 + \epsilon(1+\sigma_0^2)/(1+\sigma_0\delta_n) + O(\epsilon^2)$, where σ_0 is the spiral growth rate for $\epsilon = 0$. Pushing spirals therefore have a larger pitch than pulling spirals, as confirmed by the experiments. Experimental values of σ [Fig. 4(a)] are very well described by Eq. (6) with fitted $\epsilon = 2°$ and $\epsilon = -4°$. The fracture patterns are physical only if $\delta_n > \epsilon$. According to Eq. (2), this happens for $n < 4$ under pushing and for $n < 5$ under pulling conditions. Therefore the four-spiral pattern may be obtained in a pulling experiment, but not in the pushing case [26], as observed in our experiments (Fig. 1).

Stability of radial patterns.—We never observed radial patterns for $n = 2$ and $n = 3$, and we note that in systems that tend to favor fracture nucleation over fracture propagation [8], the final radial pattern always has at least $n = 4$ branches. However, radial fracture propagation, being symmetric, is a valid solution for any number n as it satisfies the principle of local symmetry (and the maximum energy release rate criterion). Experiments therefore suggest that the radial patterns for $n = 2$ and $n = 3$ are unstable.

It is instructive to compare the forces required for spiral and radial propagation. In Fig. 4(b), we present measurements of the force F applied on the cone along its axis during the propagation of n cracks. We find that in all cases the force is roughly constant along the experiment (see the insets), but it depends on the number n of arms. The fluctuations in the signal correspond to unexplained stick-slip fracture motion, which occur particularly in the spiraling case (see the movies in the Supplemental Material [22]).

Neglecting all variations of elastic energy, the force can be deduced by simple geometry from (1), in the radial (any n), and spiral ($n < 4$) cases (see the Supplemental Material [22]). Moreover, the self-similarity of the propagation process implies that the ratio $ds/d\rho$ is constant during one experiment, explaining why the force F is constant. We deduce the perforating forces F^r and F^s for radial and spiral propagation,

$$F^r = \frac{nG_c t\tan\gamma}{\cos(\pi/n - \alpha_c)} \quad \text{and} \quad F^s = \frac{nG_c t\tan\gamma}{\sin\psi\sin(\psi + \alpha_c - \epsilon)}, \tag{7}$$

where $\psi = \arctan\sigma$ is a function of the number of arms n [Eq. (6)]. These values are plotted in Fig. 4(b) and agree well with the experiments. Note that fracture energy G_c was found to be different in the radial and asymmetric case, probably because of a differing opening mode (see the Supplemental Material [22]). Radial propagation requires diverging forces F^r for both $n \to \infty$ and $n = 2/(1 + 2\alpha_c/\pi)$, with a minimum value for an optimal number of arms around $n = 4$, consistent with Refs. [1,8]. For $n = 2$, the spiral pattern occurs for a much lower force than the putative radial cracks, and therefore stands as a better solution. For $n = 3$, however, the radial solution would require a lower force than the spiral pattern, even though it appears to be unstable experimentally. However, the comparison of the propagation force for two different solutions (here, spiral and radial) does not provide a rigorous stability criterion. Instead, the stability of the radial fracture path should be studied directly through a perturbative analysis [27].

Conclusions.—We have shown experimentally and theoretically that multiple cracks in a thin sheet may propagate along intertwined logarithmic spiral paths building up recursively. Our approach is based on fracture mechanics and simplifying assumptions for the mechanics of very thin brittle sheets. Using the concept of recursive involutes leading to delay differential equations, we established the conditions for the existence of such structures and computed their shape and the perforating forces, in agreement with experiments. The exact mechanism by which the radial solution destabilizes and evolves towards the pattern of spirals remains, however, an open question. Multiple diverging spirals are interesting in packaging applications, where multiple tearing cracks usually lead to inconvenient convergent paths [24,28,29]. Finally, we note that the mechanics at play in such patterns is scale free and could occur at small scales, in indented graphene sheets, for instance [30,31].

J. F. F. received support from CONICYT Fellowship No. 21090746. E. H. was supported by FONDECYT Project No. 1140225. We also acknowledge support from ECOS-CONICYT Project No. C12E07 and thank N. Vandenberghe and E. Villermaux for the useful discussions.

*luis.hamm@usach.cl

[1] N. Vandenberghe and E. Villermaux, Soft Matter **9**, 8162 (2013).
[2] G. Corbett, S. Reid, and W. H. Johnson, Int. J. Impact Eng. **18**, 141 (1996).

[3] Z. P. Bazant and Y. N. Li, Int. J. Solids Struct. **32**, 303 (1995).
[4] J. Locke and J. A. Unikowski, Forensic Sci. Int. **51**, 251 (1991).
[5] T. Pfaff, R. Narain, J. M. de Joya, and J. F. O'Brien, ACM Trans. Graph. **33**, 1 (2014).
[6] N. Vandenberghe, R. Vermorel, and E. Villermaux, Phys. Rev. Lett. **110**, 174302 (2013).
[7] J. Åström and J. Timonen, Phys. Rev. Lett. **79**, 3684 (1997).
[8] R. Vermorel, N. Vandenberghe, and E. Villermaux, Phys. Rev. Lett. **104**, 175502 (2010).
[9] Y.-W. Lee and T. Wierzbicki, Int. J. Impact Eng. **31**, 1277 (2005).
[10] V. Romero, B. Roman, E. Hamm, and E. Cerda, Soft Matter **9**, 8282 (2013).
[11] D. Hull, *Fractography*, 1st ed. (Cambridge University Press, Cambridge, England, 1999).
[12] M. Sendova and K. Willis, Appl. Phys. A **76**, 957 (2003).
[13] Z. Néda, K.-t. Leung, L. Józsa, and M. Ravasz, Phys. Rev. Lett. **88**, 095502 (2002).
[14] V. Lazarus and L. Pauchard, Soft Matter **7**, 2552 (2011).
[15] J. Marthelot, B. Roman, J. Bico, J. Teisseire, D. Dalmas, and F. Melo, Phys. Rev. Lett. **113**, 085502 (2014).
[16] J. Marthelot, J. Bico, F. Melo, and B. Roman, J. Mech. Phys. Solids **84**, 214 (2015).
[17] M. L. Fender, F. Lechenault, and K. E. Daniels, Phys. Rev. Lett. **105**, 125505 (2010).
[18] B. Roman, Int. J. Fract. **182**, 209 (2013).
[19] A. Takei, B. Roman, J. Bico, E. Hamm, and F. Melo, Phys. Rev. Lett. **110**, 144301 (2013).
[20] B. Audoly, P. M. Reis, and B. Roman, Phys. Rev. Lett. **95**, 025502 (2005).
[21] B. Cotterell and J. Rice, Int. J. Fract. **16**, 155 (1980).
[22] See Supplemental Material at http://link.aps.org/supplemental/10.1103/PhysRevLett.116.165501 for movie sequences of the experiments, details of the geometrical model, and the methodology for mechanical measurements.
[23] The Lambert or omega function is defined by the complex function $W(z)$ such that $W(z)e^{W(z)} = z$, $\forall z \in \mathbb{C}$.
[24] E. Hamm, P. Reis, M. Leblanc, B. Roman, and E. Cerda, Nat. Mater. **7**, 386 (2008).
[25] T. M. Apostol and M. A. Mnatsakanian, Am. Math. Mon. **117**, 701 (2010).
[26] 4 spirals were, however, reported in perforated aluminium foils [8].
[27] I. Sivak, J. Bico, E. Hamm, and B. Roman (to be published).
[28] T. Wierzbicki, K. Trauth, and A. Atkins, J. Appl. Mech. **65**, 990 (1998).
[29] A. Atkins, Endeavour **19**, 2 (1995).
[30] D. Sen, K. S. Novoselov, P. M. Reis, and M. J. Buehler, Small **6**, 1108 (2010).
[31] C. Lee, X. Wei, J. W. Kysar, and J. Hone, Science **321**, 385 (2008).